

DESIGN OPTIMIZATION OF A TRANSONIC-FAN ROTOR USING NUMERICAL COMPUTATIONS OF THE FULL COMPRESSIBLE NAVIER-STOKES EQUATIONS AND SIMPLEX ALGORITHM

Mohamed A. Aziz¹
Institute of Aviation Engineering
and Technology
Giza, Egypt

Farouk M.Owis²
Cairo University
Giza, Egypt

Mohamed.M.Abdelrahman³
Cairo University
Giza, Egypt

ABSTRACT

In the current study, the design of a transonic-fan rotor is optimized using numerical computations of the full three-dimensional Navier-Stokes equations. The CFDRC-ACE multi physics module, which is a pressure based solver, is used for the numerical simulation. This CFD module solves the time-dependent, Reynolds-averaged Navier-Stokes equations for turbulent and compressible flows using finite volume discretization. The code is coupled with simplex optimization algorithm. The optimization process is started from a suitable design point obtained using low fidelity analytical methods that is based on experimental correlations for the pressure losses and blade deviation angle. A parametric study for the fan blade geometry is performed using the preliminary design method to find a suitable design point. The fan blade shape is defined by its stacking line and airfoil shape which are considered the optimization parameters. The stacking line is defined by lean, sweep and skews while blade airfoil shape is modified considering the thickness and camber distributions. The blade sections are defined by parametric curves so that minimum number of design variables can be considered to modify the blade shape. The optimization has been performed to maximize the rotor total pressure ratio while keeping the rotor efficiency and surge margin above certain required values. The results obtained using the CFDRC code are verified with the experimental data of Rotor 67. In addition, the results of the optimized fan indicate that the optimum design is found to be leaned in the direction of rotation and has a forward sweep from the hub to mean section and backward sweep to the tip. The pressure ratio increases from 1.427 to 1.627 at the design speed and mass flow rate.

INTRODUCTION

Transonic fans are widely used in recent aircraft engines to obtain maximum pressure ratios per stage. High stage pressure ratios are important to reduce the engine weight, size and operational costs. Performance of transonic fan has reached a high level but further improvements are required by engine manufacturers.

Recently, axial flow fans have been developed to a point where stage efficiency has exceeded 90%. The goal of the current study is to maximize the total pressure ratio and to satisfy the required efficiency and mass flow rate. High fidelity methods are used for the design optimization of transonic fans of high pressure ratios. Numerical methods offer a feasible approach to solve complex nonlinear optimization problems involving a multitude of design variables and constraints in a systematic and efficient manner. Application of this computational design optimization approaches for fan blade designs can reduce design cost, design cycle, as well as increase efficiency of jet engines [Oyama, A., Liou, L.M., and Obayashi, S. (2002)].

The problem of the design validation and optimization of transonic compressors using numerical solution of the turbulent flow equations has been under investigation by several researchers [Lian, Y., Kim, N.H., (2005), Lian, Y., Kim, N.H., (2006), and Oyama, A., Liou, L.M., and Obayashi, S., (2003)]. [Hah and Reid (1992)] conducted

¹ Ass. Teacher. In Aerospace Department, Email: mhessen_aziz@yahoo.com

² Ass. Prof. In Aerospace Department, Email: fowis@eng.cu.edu.eg

³ Prof. In Aerospace Department, Email: Dr_madbouli@hotmail.com

a numerical study based on the three-dimensional Reynolds-averaged Navier–Stokes equation to investigate the detailed flow physics inside a transonic compressor. [Ning and Xu, (2001)], performed a numerical investigation for the flow over a transonic compressor rotor using an implicit 3D flow solver with one-equation Spalart-Allmaras turbulence model.

The objective of the current study is the optimization of the rotor blade shape for a transonic fan to maximize the rotor pressure ratio while satisfying certain geometrical and performance constraints. A parametric study for the fan blade geometry is performed using a preliminary design method for transonic fans to find a suitable starting point for the high fidelity design method. Experimental correlations are used to predict the shock losses, profile losses and deviation angle during the preliminary design and off-design steps. The multiple circular arc (MCA) airfoil shape is found to be a good choice to design compressor blades during the preliminary steps.

The numerical simulations are done using the CFDRC-ACE multi physics module, which is a pressure based solver. The code solves the time-dependent, Reynolds-averaged Navier-Stokes equations for turbulent, compressible flows using a finite volume, time-marching approach on multi-zone, structured grids. Spatial accuracy is nominally second order upwind formulation. Steady flows are simulated through an iterative process using local time stepping. Turbulence is computed using the Standard $k - \varepsilon$ model.

For relative inlet Mach numbers in the order of 1.3 and higher the most important design intent is to reduce the Mach number in front of the passage shock. This is of primary importance due to the strongly rising pressure losses with increasing pre-shock Mach number, and because of the increasing pressure losses due to the shock/boundary layer interaction or shock-induced separation. The reduction of the pre-shock Mach number can be achieved by zero or even negative curvature in the front part of the blade suction side and by a resulting pre-compression shock system reducing the Mach number upstream of the final strong passage shock. The thickness is also kept very low, about 2% of chord for the tip section of a transonic fan. Besides inducing energy losses, the presence of shock waves makes transonic compressors particularly sensitive to variations in blade section design. An investigation of cascade throat area, internal contraction, and trailing edge effective camber on compressor performance shows that small changes in mean line angles, and consequently in the airfoil shape and passage area ratios, significantly affect the performance of transonic blade rows [Wadia AR, Copenhaver WW. (1996)].

One of the most important airfoil design parameter affecting the aerodynamics of transonic blading is the chord wise location of maximum thickness. Good performance is obtained for the lower shock front losses with the finer section which results when the location of the maximum thickness is moved aft. An optimum maximum thickness location is assumed to exist in the range of 55% to 60% of the chord length for transonic fan rotors [Roberto Biollo, Ernesto Benini , (2013)]. Not only the position of maximum thickness but also the airfoil thickness has a significant impact on the aerodynamic behavior of transonic compressor rotors.

The flow field in a compressor is not only influenced by the two-dimensional airfoil geometry. The three-dimensional shape of the blade is also of great importance, especially in transonic compressor rotors where an optimization of shock structure and its interference with secondary flows is required. Many experimental and numerical studies have been done for the design and analysis of three-dimensional shaped transonic blading (e.g., [Hah C, Rabe DC, Wadia AR., (2004)] and [Puterbaugh SL, Copenhaver WW, Hah C, Wennerstrom AJ., (1997)]).

MATHIMATICAL MODEL

An optimization algorithm is used to maximize the total pressure for the fan rotor blades using the CFD-RC package. The rotor blade geometry is parameterized in order to facilitate its handling through the design process. The level of success in parameterizing the blade is dependent on two factors. First factor is the flexibility and amount of coverage of all possible solutions. The second factor is the compactness of the parameters. The more accurate the description of the blade the bigger the number of parameters needed. The optimization process is used to determine the following dimensions:

- Thickness distribution of each section at different radii.
- Camber distribution of each section at different radii.
- Staking line of the different blade sections from hub to tip.
- Blade twist distribution over the staking line.

Classification of design optimization parameters. The pre-mentioned design parameters are the factors affecting blade shape optimization process. They can be classified into two main groups. First group is the hub-to-shroud (z-r or meridional) plane group. Second group is the blade-to-blade ($r-\theta$) plane group and the mixing

between blade-to-blade and hub-to-shroud planes group. In the following sections the details of each group are described and their effects on the rotor blade performance are investigated.

Hub to shroud plane group. The Hub-to-Shroud (meridional) plane group geometry is parameterized as follows,

- 1) Blade inlet and exit hub radius.
- 2) Blade inlet and exit tip radius.
- 3) Equation describing the hub curve in the meridional plane.
- 4) Equation describing the tip curve in the meridional plane.

This classification is based on the direct physical dimensions and their effect on the fan performance. Inlet hub and tip radii together are affecting the inlet area and so the average inlet Mach number. The inlet tip radius effects the peripheral speed consequently, the value of relative Mach number at the tip, which should be kept as low as possible to minimize losses in this part. The equations describing the hub and tip curves in the meridional plane can affect the pressure gradient on the hub and tip surfaces, boundary layer growth and the associated velocity profile. It is difficult to manipulate these parameters efficiently using simple 1-D or even 2-D models. It should be manipulated using 3-D CFD solvers to account for its different impacts on the flow. The meridional plane group is shown in Figure 1.

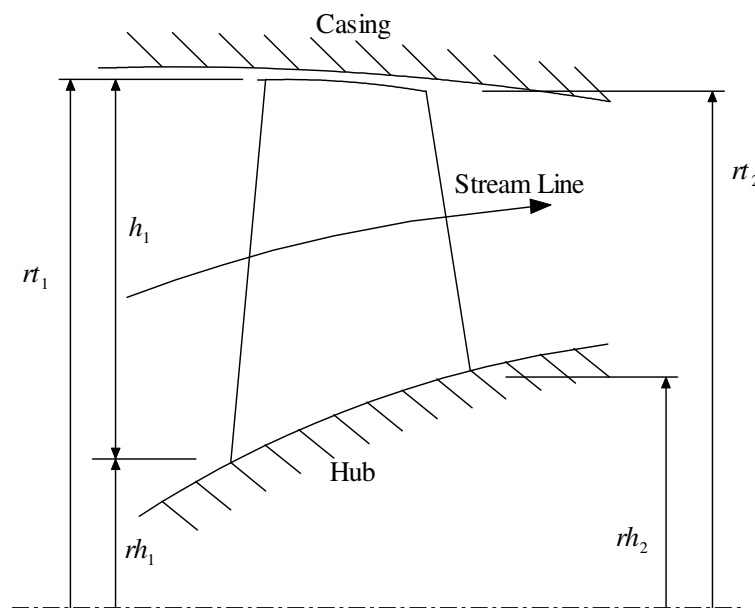


Figure 1: Hub-to-shroud (meridional) plane group.

Blade to blade plane group. The blade to blade plane geometry is parameterized as follows,

- 1) Blades spacing.
- 2) Equation describing the mean blade camber line.
- 3) Equation describing the blade thickness distribution along meridional coordinates.
- 4) Blade chord distribution.
- 5) Stagger angle.

The first parameter (blades spacing) depends on the number of blades, and the radius at this location. Its combined effect with the second, third parameters and blade height determines the choking conditions. The blade camber, thickness distribution and the stagger angle determines the blade inlet and exit angles. The blade inlet angle affects directly the velocity triangle at the inlet, flow incidence angle, and relative Mach number. The exit blade angle affects the work of the rotor, through affecting the circumferential absolute exit velocity. Figure 2 shows the blade-to-blade plane group.

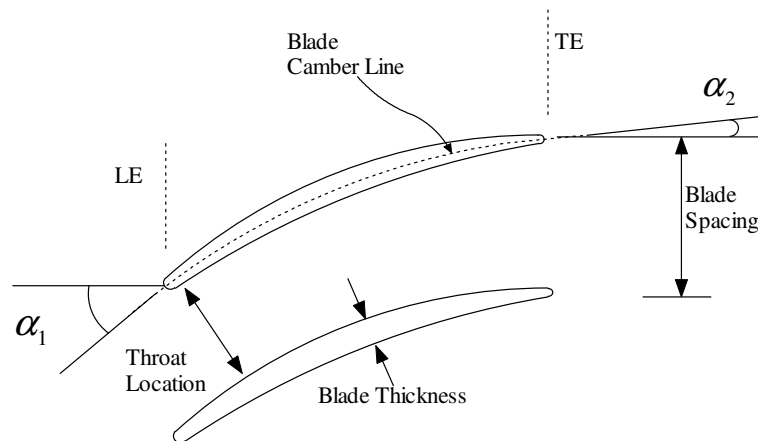


Figure 2: Blade to blade plane group.

Mixing between blade-to-blade and Hub-to-shroud planes group. It is a set of geometry parameters that may appear in the two planes described above. It could be parameterized as follows,

- 1) Equation describing the axial position of the section staking point over the radial direction.
- 2) Equation describing the circumferential position of the section staking point over the radial direction.

The first parameter (staking point axial coordinates), which should cause the blade to sweep back or forward. This sweep has its effect in improving the blade adiabatic efficiency as mentioned by [Choon-Man, PingLI, and Kwang-Yong KIM, (2005)]. A recent numerical and experimental work showed that the axial blade curvature can help to influence the shock shape in the meridional plane, inducing the shock to assume the meridional curvature of the blade leading edge. In addition, a considerable impact on the radial outward migration of fluid particles which takes place inside the blade suction side boundary layer after the interaction with the shock has been confirmed. Numerical and experimental analyses carried out to evaluate the performance of a forward swept rotor and an aft swept rotor showed that the forward swept rotor had a higher peak efficiency and a substantially larger stall margin than the baseline unswept rotor, and that the aft swept rotor had a similar peak efficiency with a significantly smaller stall margin [Hah C, Puterbaugh SL, Wadia AR., (1998)].

Detailed analyses of the measured and calculated flow fields indicated that two mechanisms were primarily responsible for the differences in aerodynamic performance among these rotors. The first mechanism was a change in the radial shape of the passage shock near the casing by the end wall effect, and the second was the radial migration of low momentum fluid to the blade tip region. Similar results were obtained in a parallel investigation which identified the reduced shock/boundary layer interaction, resulting from reduced axial flow diffusion and less accumulation of centrifuged blade surface boundary layer at the tip, as the prime contributor to the enhanced performance with forward sweep [Wadia AR, Szucs PN, Crall DW., (1998)].

The second parameter (staking point circumferential coordinates), which should cause the blade lean. As mentioned in [Bergner J, Kablitz S, Hennecke DK, Passrucker H, Steinhardt E., (2005)] and [Kablitz S, Passrucker H, Hennecke DK, Engber M., (2003)], it is weakening the passage's shock and is reducing loss core near the tip of the suction surface. A recent numerical work gave a point of view on the impact of blade curvature in transonic compressor rotors, showing how the movement of blade sections in the tangential direction can influence the internal flow field [Benini E, Biollo R., (2007)] and [BiolloR, Benini E., (2008)]. Another research group investigated the aerodynamic effects induced by several tangential blade curvatures on the same rotor. It was observed that when the curvature is applied towards the direction of rotor rotation, the blade-to-blade shock tends to move more downstream, becoming more oblique to the incoming flow. This reduced the aerodynamic shock losses and entropy generation, showing in some cases a peak efficiency increment of over 1% at design speed [Benini E, Biollo R., (2008)]. Similar results were previously obtained using a numerical optimization algorithm [Ahn C-S, Kim K-Y., (2002)].

Higher performance can be achieved using a proper combination of two orthogonal blade curvatures, i.e., the use of a blade curved both axially and tangentially, as well as swept and leaned at the same time as applied in the current study. Figure 3 shows the blade-to-blade and plane group hub-to-shroud planes mixing group.

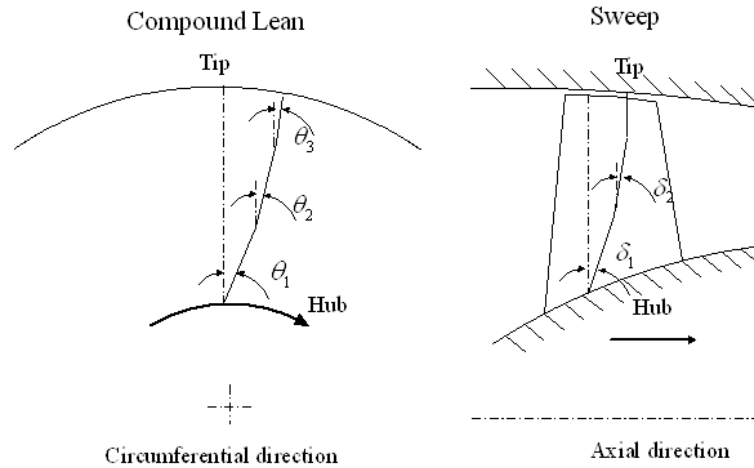


Figure 3: Definition of swept and leand rotor blade geometry.

Blade thickness distribution and camber line curve treatment. The blade camber line curve has a major role in the design problem. It describes the blade angle distribution along the meridional path. The inlet and exit blade angles effect directly the work transferred to the fluid. Describing the camber line could be done using polynomial or Bezier curves. Five or six points Bezier curve are sufficient to describe a complex curve, where a polynomial of higher order is needed to do the same job. In the present work, three sections are defined, each section is defined using five points Bezier curve for description of the camber line curve. That is to say, if every point has two coordinates (x, y) , a total number of (30) variables need to be defined. Figure 4 shows the Bezier points used for description this curve. In the present work, and for the purpose of simplicity, the number of sections considered is only three sections, where the more sections are more recommended. The meridional coordinates are taken as (0%, 25, 50%, 75%, 100%) of the chord length with the first and last point are fixed.

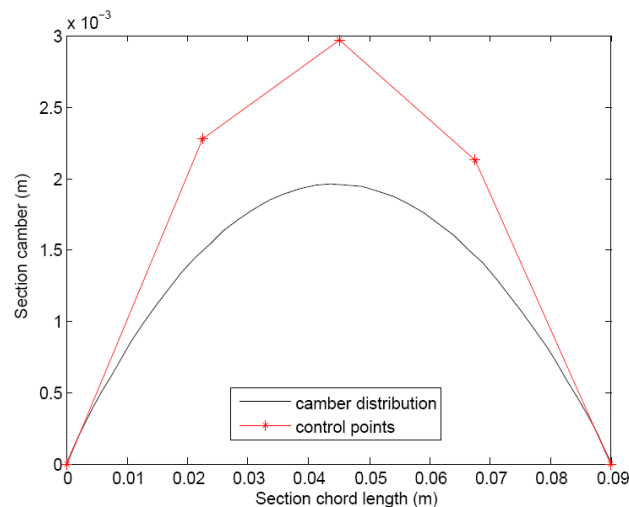


Figure 4: Bezier curve describing blade camber line.

The blade thickness distribution along the meridional coordinates could be described using polynomial or Bezier curve. In present work this parameter was investigated using seven points Bezier curve. Where, the coordinates of the second and six points in the meridional directions represent the leading and trailing edges radiuses. The remaining points are treated as described above in the camber line treatment. Figure 6 shows a typical blade thickness distribution, using Bezier curve of figures 4, 5.

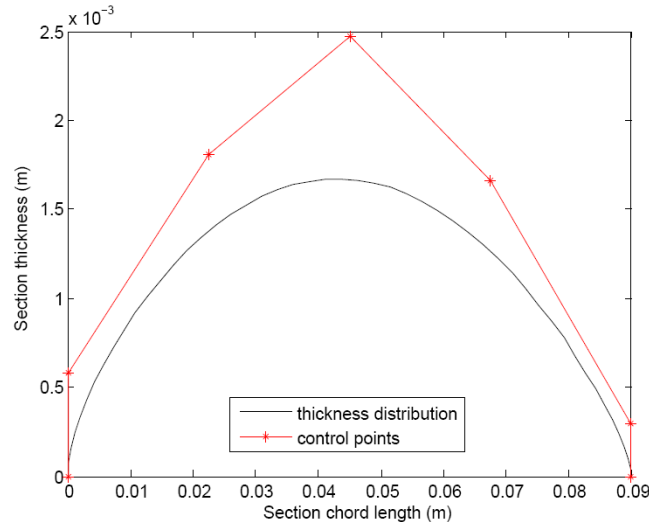


Figure 5: Bezier curve describing blade thickness distribution.

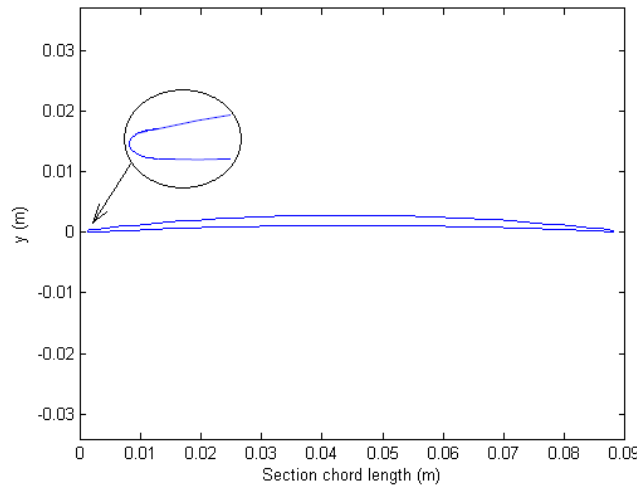


Figure 6: Typical blade thickness, and blade camber line in blade to blade plane using Bezier curve.

Section thickness and camber representation. In order to start the optimization for the section thickness and camber distributions the Bezier control points should be determined. A Bezier curve is defined by a set of control points P_n where n is the order. A Bezier curve with 5 control points is a fourth order curves. The parametric curves may be defined as follows,

$$y(x) = \sum_{i=0}^n b_{i,n}(x)P_i, x \in [0, 1] \quad (1)$$

where the control points is P_i and $b_{i,n}(x)$ are polynomials defined as,

$$b_{i,n}(x) = \binom{n}{i} x^i (1-x)^{n-i} \quad (2)$$

and the $\binom{n}{i}$ is the binomial coefficient defined as,

$$\binom{n}{i} = \frac{n!}{i!(n-i)!} \quad (3)$$

There are different methods to find the control points coordinates that accurately represent the section camber and thickness distributions. One method that gives accurate results is that using optimizations algorithm. The algorithms used to locate the control points with the best fitting to the original curve. Figure 7 is a representation for applying the Particle Swarm Optimization (PSO) [Qinghai Bai,,(2010)] on the camber line curve of a famous NACA rotor 67.

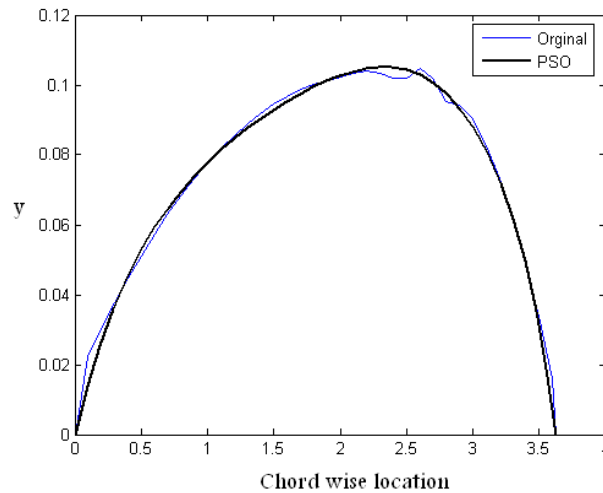


Figure 7: Bezier 5 control points representation for the camber line obtained by PSO

In spite of that, the previous discussion was investigating, the effect of different parameters on the performance of the rotor blade. The actual behaviour of the rotor blade is affected by the combination of the geometrical parameters together, not by everyone alone. That limits the ability of trusting empirical, and simple one dimensional equations result. In addition, forces the designer towards the obligatory 3-D CFD solution, which deals with the actual geometry as one unit, combining all the previously mentioned points. After the previous parameterization, the blade is looks like a paste. The variation of the coordinates of any geometric parameter will lead to a new geometry. Now it is easy to manipulate the problem using an optimizer.

THE CFD CODE

The CFD analysis or simulation is highly dependent on the boundary conditions because the flow is internal and the boundary conditions are applied in proximity to the complex flow features. The first objective of this section is to describe the subsonic inflow and outflow boundary conditions that have been implemented into the CFD code and applied for the analysis of flows through transonic fans. The second objective is to validate the utilized CFD code CFD-ACE through a comparison of the results with the computational and the experimental work done.

The CFDRC- ACE multi physics module, which is a pressure based solver. It solves the time-dependent, Reynolds-averaged Navier-Stokes equations for turbulent, compressible flows using a finite volume, time-marching approach on multi-zone, structured grids. Spatial accuracy is nominally second order upwind formulation. Steady flows are simulated through an iterative process using local time stepping. Turbulence is modeled using the Standard $k - \epsilon$ model [Lauder, B. E. and Splading, D. B., (1972)]. CFD-ACE is capable of solving flows of speeds ranging from low subsonic flow to relatively high supersonic flow.

Standard boundary conditions for subsonic flows are implemented. At the inlet, the flow angles, total pressure, velocity and total temperature are specified. At the outlet, the average value of the static pressure at the hub is prescribed, whereas circumference pressure gradient is extrapolated to maintain a specified average static pressure. The density and velocity components are extrapolated from interior. On the solid wall, the temperature is set constant as the total temperature at the inlet and the pressure is extrapolated from the interior. The no-slip boundary conditions and the temperature condition are used together to compute the density and total energy. Periodic boundary conditions are applied from blade to blade passage. Figure 8 is a representation of the boundary conditions specified in the problem. Initially, the flow properties in the computational domain are assumed to be uniform and are set equal to the inlet free stream values.

The tip clearance region is handled by the periodic condition across the blade. The tip clearance region is included in the computations using an additional patch of grid. In addition, for the similar rotors (rotor67), it is found that the tip clearance effect becomes important only when the stall condition approaches [Lian, Y., Kim, N.H., (2005)]. In the current study, it is considered to be a good representation of the flow without gridding up the tip region.

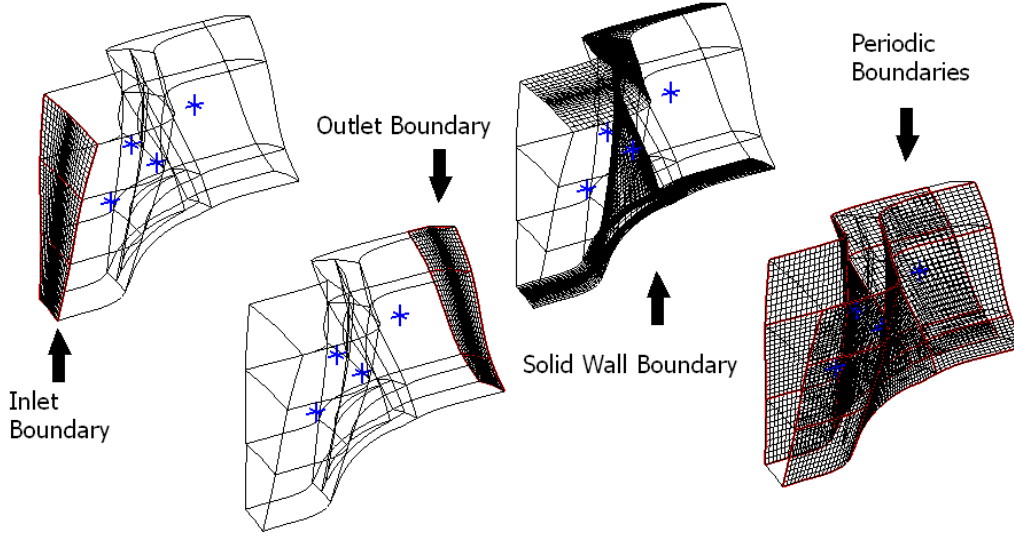


Figure 8: Boundary conditions.

The grids used in the simulations are generated using characteristic grid spacing, h . The finest grid spacing is denoted as, h_1 . For each grid, the simulation results in an observed flow quantity, f , such as the total pressure ratio. The change in the quantity f between the grids is expressed in terms of the grid convergence index (GCI). GCI error estimates can be used with minimum of two mesh solutions but provide a better error estimate when used with three mesh solutions [Roache, P.J., (1994)]. The GCI between a finer grid with spacing h_1 and coarser grid with spacing h_2 is defined as,

$$GCI = \frac{F_s \left| \frac{f_2 - f_1}{f_1} \right|}{r^p - 1} \quad (4)$$

Where r is the refinement ratio between the finer grid and coarser grid and p is the order of grid convergence observed in the simulations, and are given by

$$r = \frac{h_2}{h_1} \quad (5)$$

$$p = \frac{\ln\left(\frac{f_3 - f_2}{f_2 - f_1}\right)}{\ln(r)} \quad (6)$$

A factor of safety of $F_s = 1.25$ is based on experience applying GCI in many situations [Roache, P.J., (1994)]. A second-order solution would have ($p=2$). The GCI is a measure of the percentage difference of the computed quantity from the value of the asymptotic numerical value. It approximates an error band and indicates how much the solution would change with further refinement of the grid. Verification assessment involves performing consistency checks. One such check is that mass is conserved through the flow domain. For inlets and ducts, mass conservation can be assessed spatially along the stream wise coordinate of the duct. Mass flow bookkeeping tracks the mass flow through the compressor with that of the captured mass flow. The boundary conditions are indirectly verified through comparison of the simulation results to available analytic results for the flow field. The geometry and grid generation for rotor blade constructed at the geometry module.

A grid sensitivity study is performed to ensure that the baseline grid has adequate sizes to resolve the solid wall boundary layers and the shock system. Simulations are conducted on different grids with variable grid points. Table 1 summarizes the sensitivity of the number of cells for structured grids Fig. 9. Figure 10 shows the variation of the observed flow quantity (i.e. total pressure ratio) for different grids sizes of the first grid point near the wall. Figure 11 shows the convergence history of the normalized mass flow rate ($\dot{m} / \dot{m}_{Design}$) through the rotor for the current considered grid. The computations asymptotically converge after 750 iterations to same design mass flow rate.

Table 1: Rotor pressure ratio for different grid sizes.

No. of Cells	2E5	5E5	8E5	10 E5
1 st grid spacing (meter)	8.0E-4	3.5E-4	3.0E-4	2.5E-4
(Stage Total Pressure Ratio)	1.426	1.4317	1.4327	1.4334

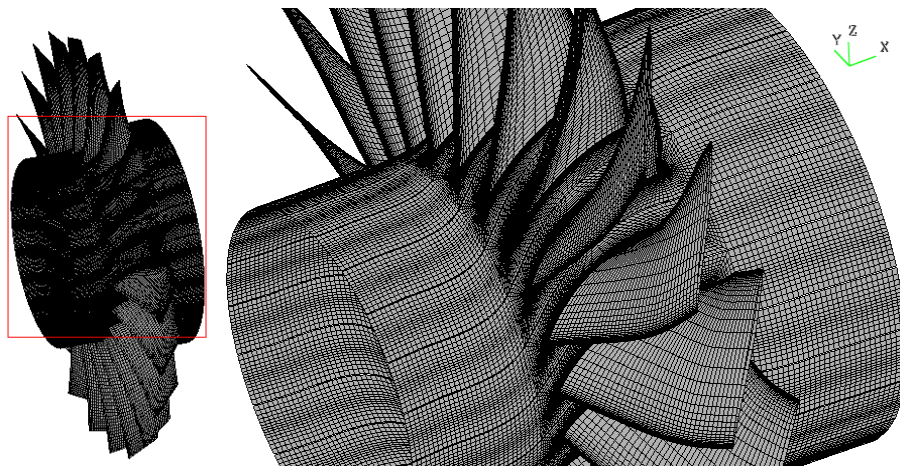


Figure 9: Fan rotor structured grid.

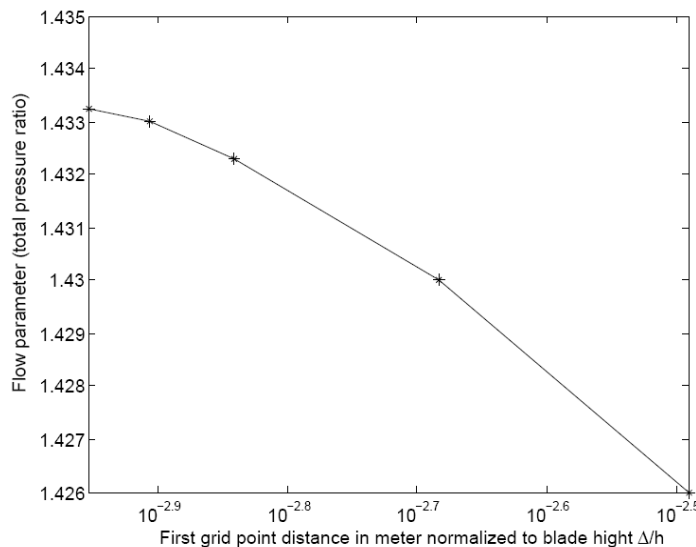


Figure 10: Effect of grid spacing on the accuracy of the steady state solution

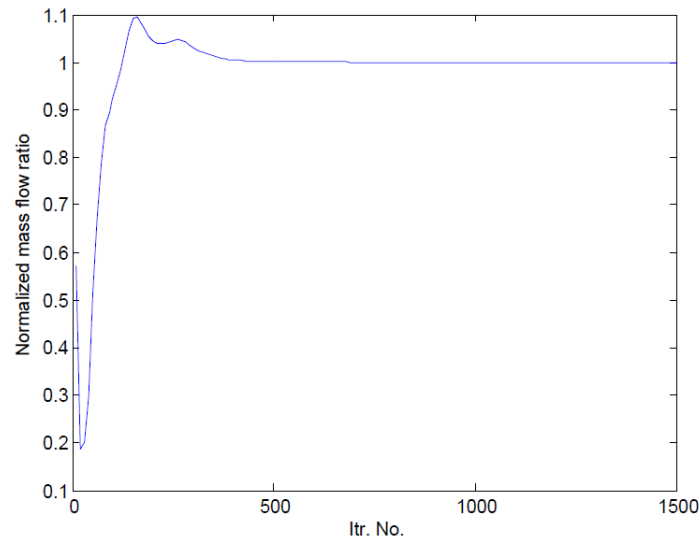


Figure 11: Non-dimensional mass flow rate convergence history.

HIGH FIDELITY OPTIMIZATION

The aim of the present study is to obtain an optimum blade geometry for a given preliminary design of the transonic fan with some geometrical and performance constraints. The final task is to combine all the developed modules in association with the SIMPLEX optimization algorithm to complete the optimization cycle. Figure 12 illustrates the sequence of the optimization flowchart with some modifications.

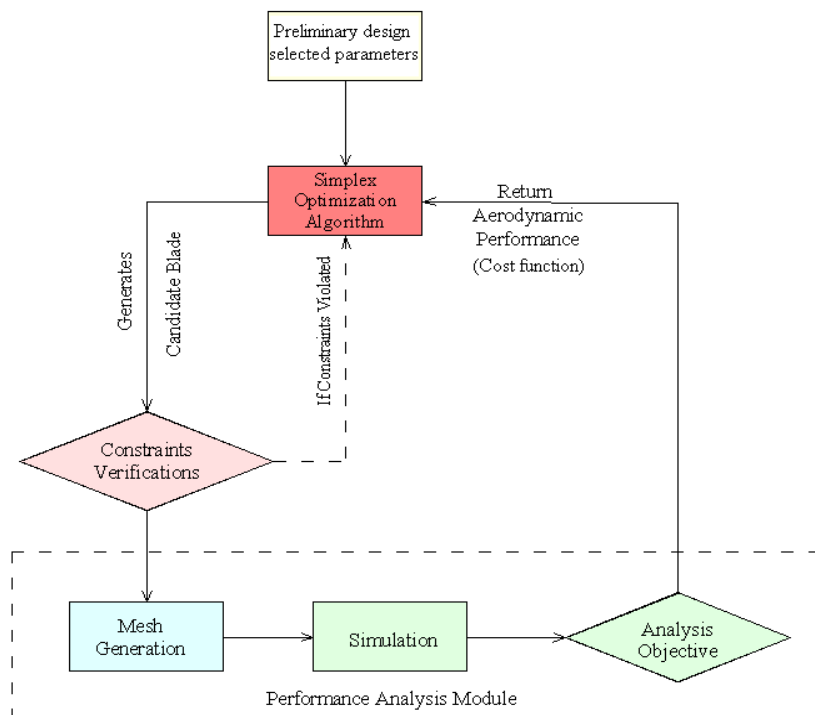


Figure 12: A flowchart for the design optimization process.

Optimization algorithm. The simplex algorithm is used for the optimization process. The algorithm is a direct (non-gradient) optimization method and requires only one objective function evaluation per design iteration. The algorithm is robust and is likely to converge. The algorithm is easy to use because it has only three parameters to adjust (initial values of variables, first step size and minimum and maximum variables values). Some of the algorithm disadvantages are that as with most algorithms, the algorithm may find a local minimum instead of the global minimum. Different minimum

solutions can be found by starting the optimizer at different initial points. Since the Simplex algorithm does not use past information to accelerate movement through the design space, convergence can be slow (especially with a large number of design variables).

A simplex is a polygon defined by $(n+1)$ vertices in n -dimensional space. For example, in 2D, a simplex is a triangle, Fig. 13. The simplex is termed "regular" if its vertices are equidistant. Each vertex of the polygon represents a single design configuration, with design variable values $X(1), X(2), \dots, X(N)$ each corresponds to an objective function value. To progress towards an optimum solution, the simplex algorithm reflects the vertex associated with the worst design through the centroid of the polygon. New design variable values and the associated objective function value define the new point. As the algorithm progresses through the design space, two setbacks can occur. The first setback if current worst design is created in the previous iteration. If this point is again reflected, the algorithm would bounce back and forth between two configurations. The algorithm instead reflects the second worst point. The simplex moves in a different direction, away from the stall point. An objective function that has a steep valley leading to a local minimum will cause the Simplex algorithm to cycle infinitely through the same design points at the rim of the valley. The second setback is when simplex cycles through the same designs over a period of several iterations, the algorithm is stalled. Reducing the physical size of the simplex allows it to fit into the valley and get closer to the minimum solution. The size reduction is done at the first instance of a repeated design.

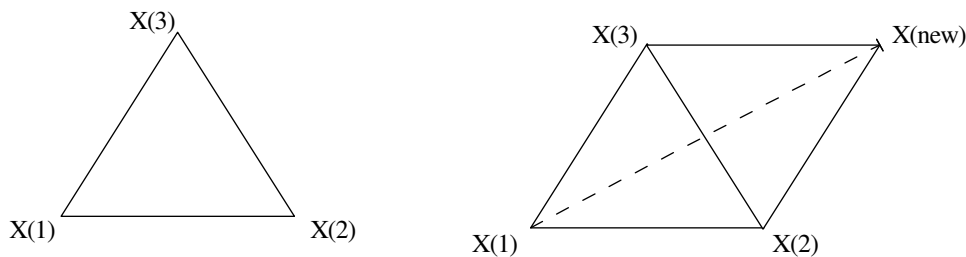


Figure 13: New Design Point in Simplex Optimization Algorithm.

An initial value for each design variable must be specified. The optimizer uses initial variable-values as a starting guess for the optimization studies. These values will be used to create the first design. To start the optimization process, one must enter a value for the first step. This value essentially sets the geometric size of the Simplex and affects the behavior of the algorithm. A good rule of thumb for choosing a value for Delta is 20% of the size of the entire design space. For each design variable enter the minimum and maximum allowable design variable values (constraints). This will bound the optimizer, preventing it from choosing designs that lie outside this range. Constraints are useful for preventing creation of unrealistic geometry or application of unrealistic boundary or volume conditions. The maximum and minimum values were set as $\pm 10\%$ for most of the variables such Bezier points coordinates. This cycle is segmented into main steps that was previously developed and programmed. They are as follows,

- The low fidelity (preliminary design) is started and the geometry of the new design specified.
- The simplex optimization algorithm starts with the low fidelity optimal as a base line of optimization
- The geometry construction variables are imported in CFD-GEOM and geometry is constructed, then the constructed geometry will pass through the constraint verifications stage. In this stage the geometry is checked to make sure that it satisfies the geometry constraints. Then, the edge grid is generated, all steps being carried out by executing the developed Grid Generation module.
- The boundary condition, initial condition, and solver controls are applied in the simulation module by executing the Solver Setting module.
- Then, the analysis objective module executes. Output of this module is a data file containing values, which is the average value of the cost function and the geometric parameters.
- The simplex optimizer continues to run on the other geometry, and the path of the optimization is stored in a data file to monitor the history of results during the optimization run.

All the above steps are arranged and programmed using the PYTHON language and conducted in the Simulation Manager module, which is one of the modules in the CFDRC package.

RESULTS

Low fidelity design results. The baseline data of the selected transonic fan is presented in Table 2. This baseline data is used during the preliminary design phase. The results of the preliminary design using low fidelity module are presented in Table 3. The initial estimation of the number of stages indicates that 3 stages are required to obtain the required overall pressure ratio. A parametric study is performed to investigate the effect of different design parameters on the fan performance and to choose the design parameters such as the rotational speed, blade geometry and the stagger angle of the rotor and stator. The fan performance is computed in terms of the surge margin, fan efficiency and pressure ratio at the design and off-design conditions as shown in Fig. 14. The selections, that are based on minimum number of stages with maximum isentropic efficiency, allow producing the required fan pressure ratio. The three stages fan is the result of compromise between the isentropic efficiency and tip speed constraint. The fan stages have pressure ratios of 1.55, 1.36 and 1.25 for the 1st, 2nd, and 3rd stages respectively.

Table 2: Base line data of the selected case.

Requirements		Inlet Conditions		Selected Parameters	
Mass flow rate	120 kg/sec	Total inlet temperature	300 K	N (r.p.m)	<10500
Fan pressure ratio	2.6	Total inlet pressure	101.325 kPa	Hub to tip ratio	0.2-0.7
				Diffusion Factor	<0.55
				Inlet axial Mach Number	0.7

Table 3: Low fidelity design parameters

Parameter	First Stage		Second Stage		Third Stage	
	Rotor	Stator	Rotor	Stator	Rotor	Stator
Blades Number	25	27	34	35	34	35
Mean radius (m)	0.32	0.32	0.32	0.32	0.32	0.32
Aspect ratio	3.45	3.15	4	3.8	3.5	3.55
Blade height	0.28	0.21	0.2	0.19	0.17	0.16
Hub/tip ratio	0.39	0.49	0.52	0.53	0.57	0.6
(r.p.m)	9,800	-	9,800	-	9,800	-
Tip speed (m/s)	450	-	411.3	-	398	-
M_{rel} at tip	1.63	-	1.15	-	1.08	-
Pressure ratio	1.55		1.36		1.25	
Isentropic eff.	0.944		0.9337		0.9052	

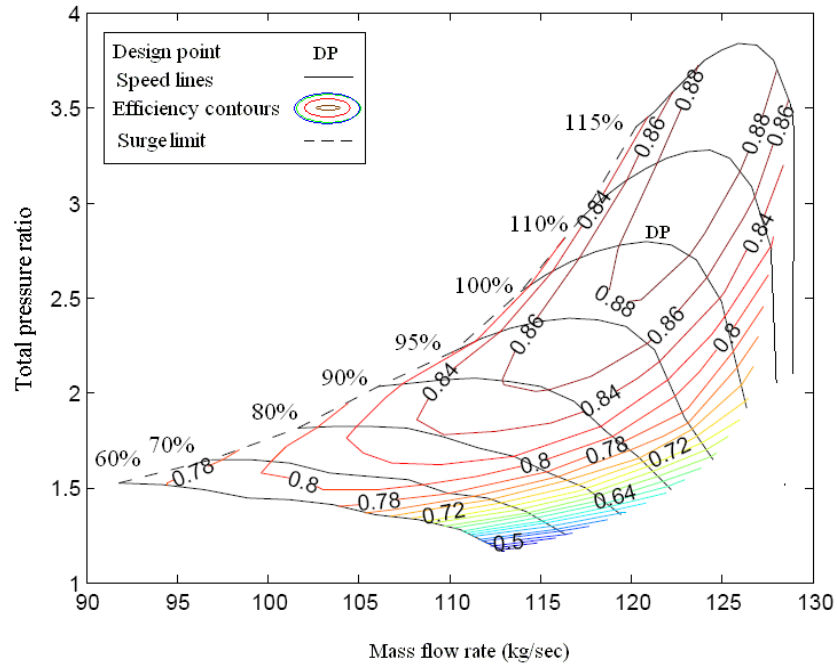


Figure 14: Low fidelity fan performance map

High fidelity design results. Running the high fidelity cycle optimizer, the problem converges to an optimal design. The history of the optimization process is shown in Figure 15 and the results for the optimization are presented in Table 4 for the sake of comparison with the numerical results of the low fidelity design. The results show an increase of total pressure ratio by 13.8% and the isentropic efficiency increases as well. The number of blades is reduced by 3 blades from the original low fidelity design.

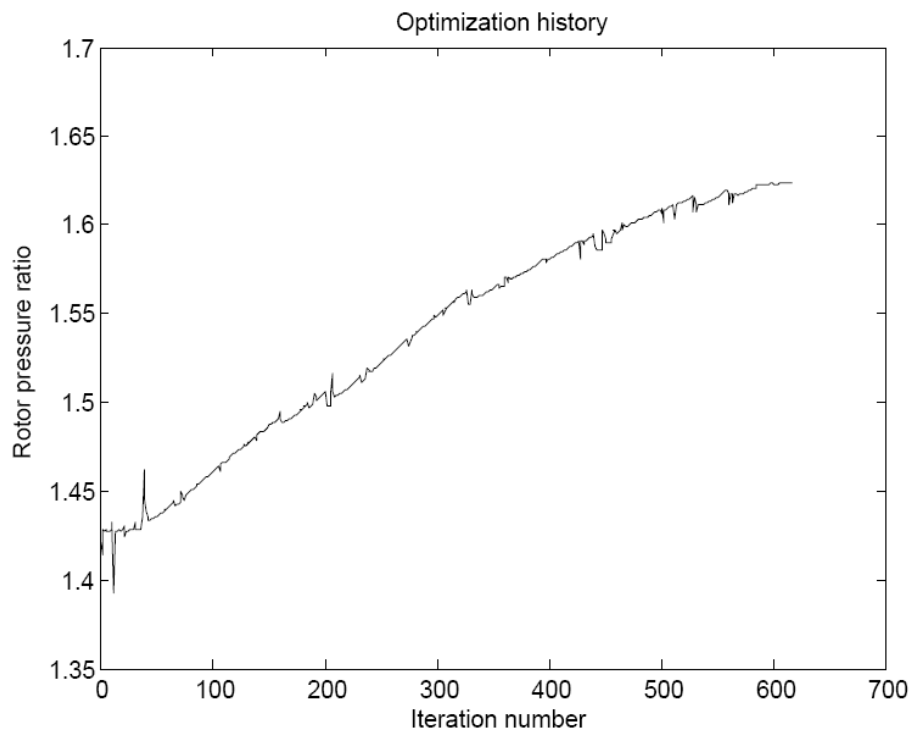


Figure 15: Variation of the rotor pressure ratio during the optimization process.

Table 4 Rotor design performance

Parameter	Low fidelity design	High fidelity design
Pressure ratio	1.43	1.627
Isentropic efficiency	0.82	0.842
Leaned	Non	In direction of rotation
Swept	Non	Forward swept (hub to mean) Backward Swept (mean to tip)
Numbers of blades	25	22

The high fidelity design is found to lean toward the direction of rotation. The rotor blade is swept forward from the hub to mean portion of the blade and have a backward swept for the rest of the blade Fig. 16. Previous study [Roberto Biollo, Ernesto Benini , (2013)] concludes that more leaned rotor blade increases the rotor isentropic efficiency and the operating range. The forward swept rotor is found to have higher peak efficiency and a substantially larger stall margin than the baseline of non sweep rotor.

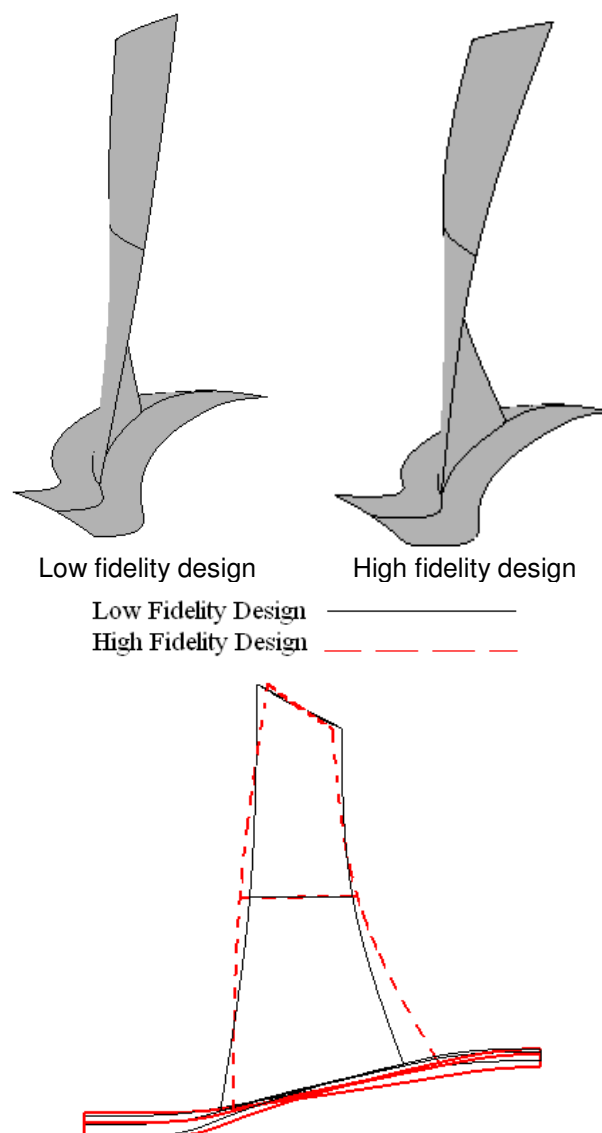


Figure 16: Comparison between high fidelity design and low fidelity design blade shape.

With the large number of optimization variables, there is a difficulty to detect the effect of each variable alone on the high fidelity design performance. One may conclude many observations from Fig. 17. The blade chord length tends to increase at the hub section and the stagger angle slightly

increases too. At the mean section the chord increases while the stagger angle remains almost constant. The tip section has a greater stagger angle with a shorter chord length than the low fidelity design.

Table 5 shows the axial flow compressors characteristic in the different flow regimes. Similar transonic stages with inlet Mach number from 0.7 to 1.1 limited by a pressure ratio from 1.15 to 1.6 and an isentropic efficiency from 80% to 85% are obtained. The isentropic efficiencies decrease with the increase of the inlet relative Mach number. The current transonic rotor produces a pressure ratio of 1.62 with absence of the stator. With the complete stage this pressure ratio should slightly decrease due to the pressure loss.

Low Fidelity Design —————
 High Fidelity Design - - - - -

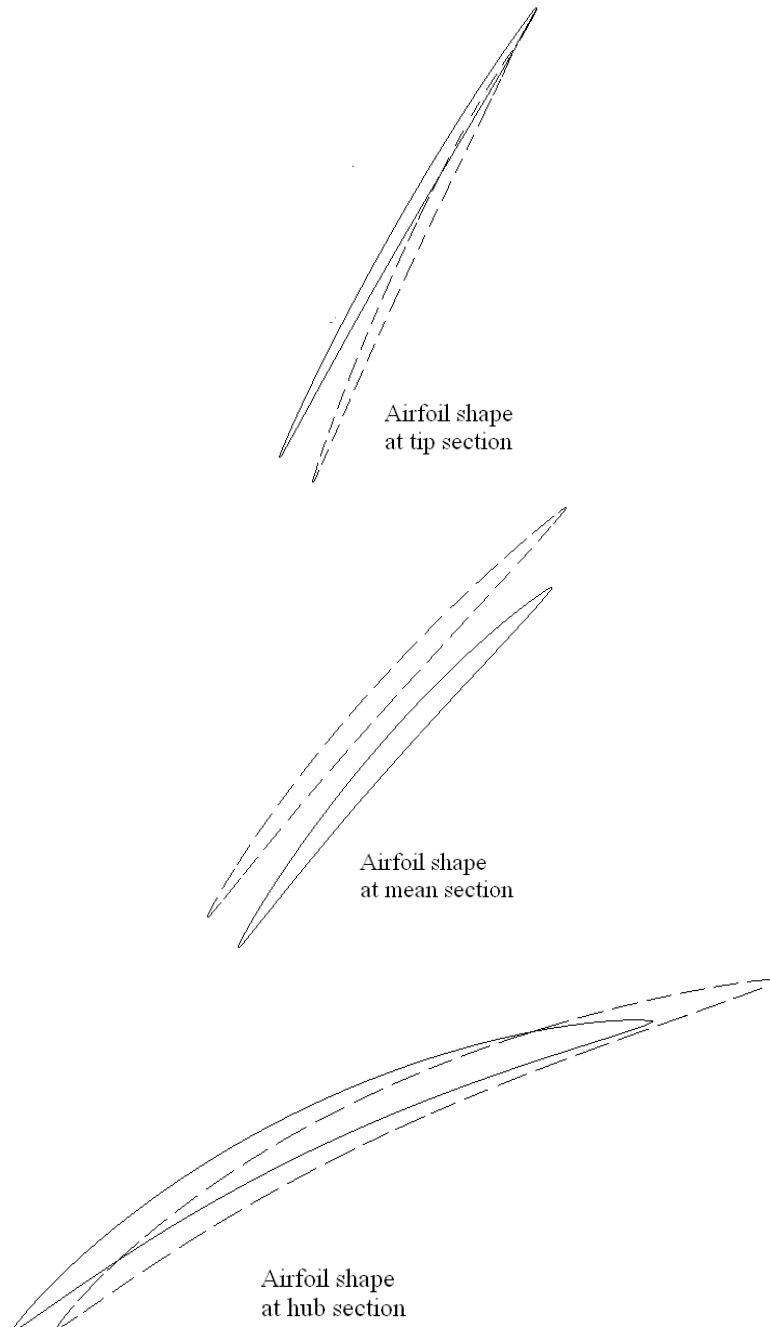


Figure 17: Comparison between low fidelity design and high fidelity design airfoil shape at 0%, 50% and 100% span from hub.

Table 5: Axial Flow Fan Characteristics [Boyce, M.P,(2003)].

Type of Application	Inlet Relative Mach Number	Pressure Ratio	Efficiency
Industrial (Subsonic)	0.4-0.8	1.05-1.2	88%-92%
Aerospace (Transonic)	0.7-1.1	1.15-1.6	80%-85%
Research (Supersonic)	1.05-2.5	1.8-2.2	75%-85%

The total pressure contours at the inlet and exit planes of the rotors are presented in Fig. 18. The high fidelity design has a high pressure distribution near the hub region than the low fidelity one.

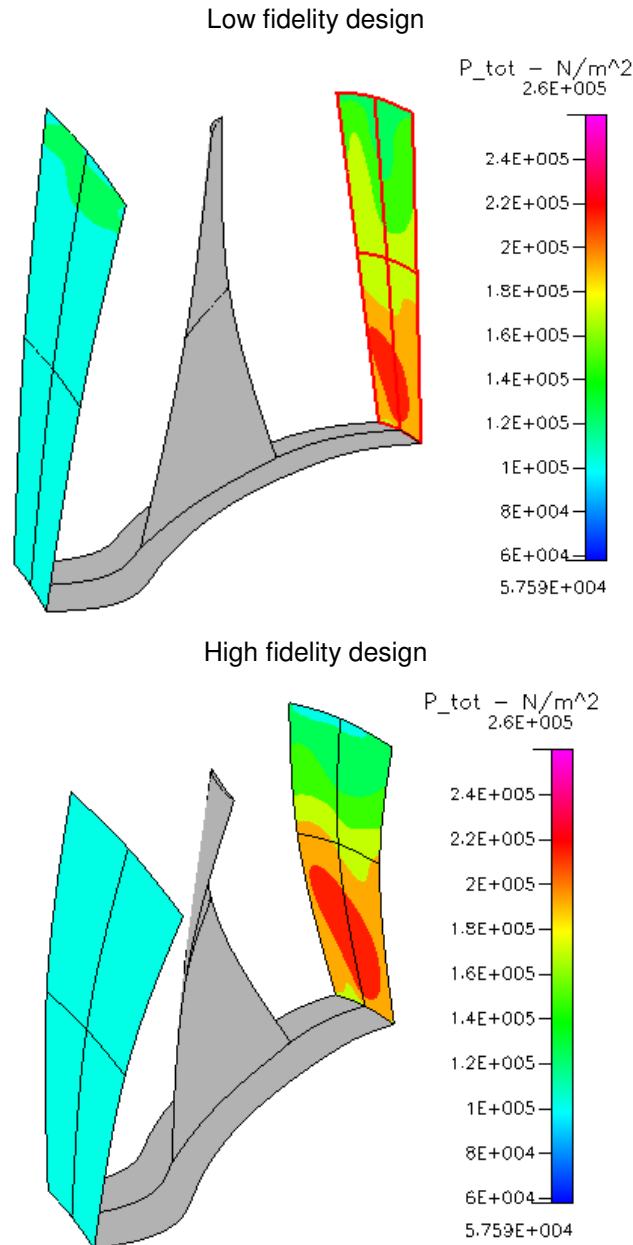


Figure 18: Comparison between total pressure contours for high fidelity and low fidelity designs.

The high fidelity design Mach number contours at the mean section are compared to those of the low fidelity and they are presented in Fig. 19. The high fidelity design has a lower Mach number in front of the passage shock. Thus the losses across the shock are reduced and the passage shock is moved toward the blade leading edge. The shock system inside the passage is reduced to one strong shock. Researchers explain the shape of the shock at the peak efficiency operation as an oblique

shock followed by normal shock [Keith M. Boyer, (2001)] and [Gregory S. Bloch, (1996)]. The location of the normal shock is controlled by the back pressure applied to the rotor.

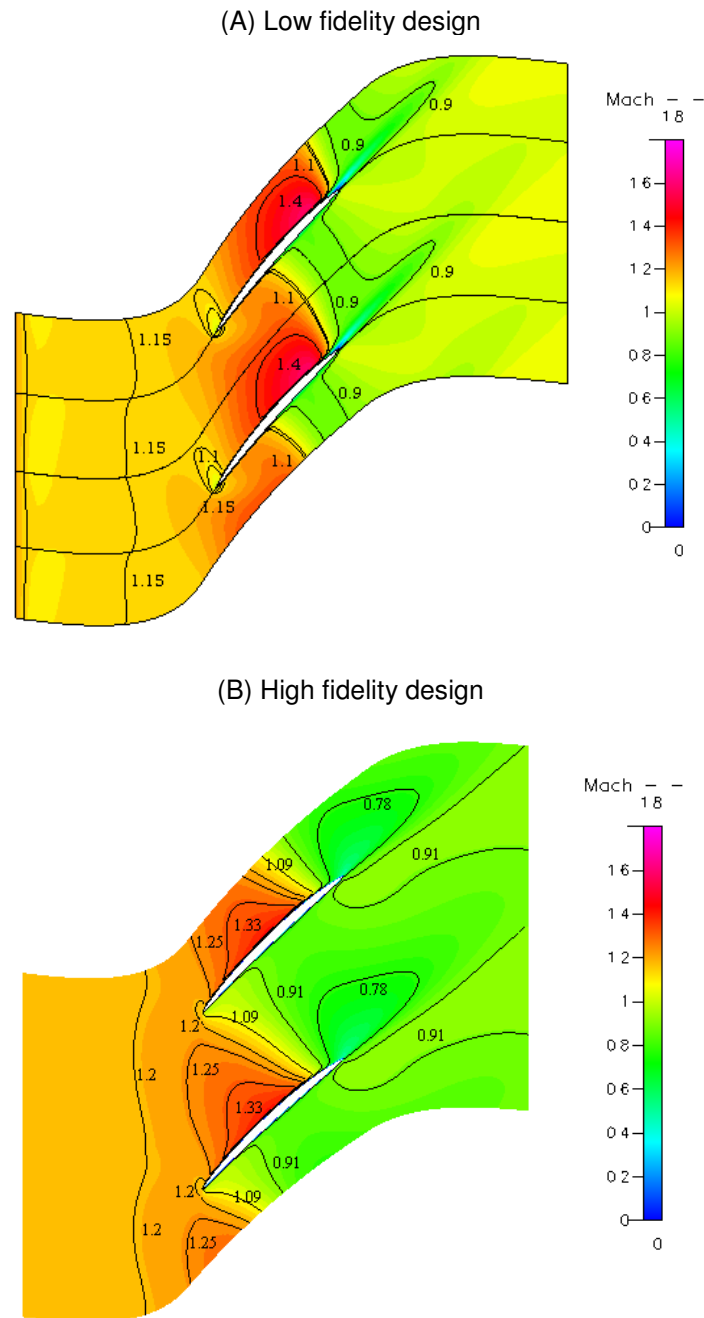


Figure 19: Comparison between high fidelity design and low fidelity design Mach contour at mean, near the hub, and tip sections.

The same observations are shown in Fig. 20 (A) near the hub section. Near the tip section Fig. 20 (B) the flow enters the passage with relative Mach number of about 1.4. The Mach number in front of the shock reaches 1.55 which reduces to 0.95 after the shock.

(A) Near hub section

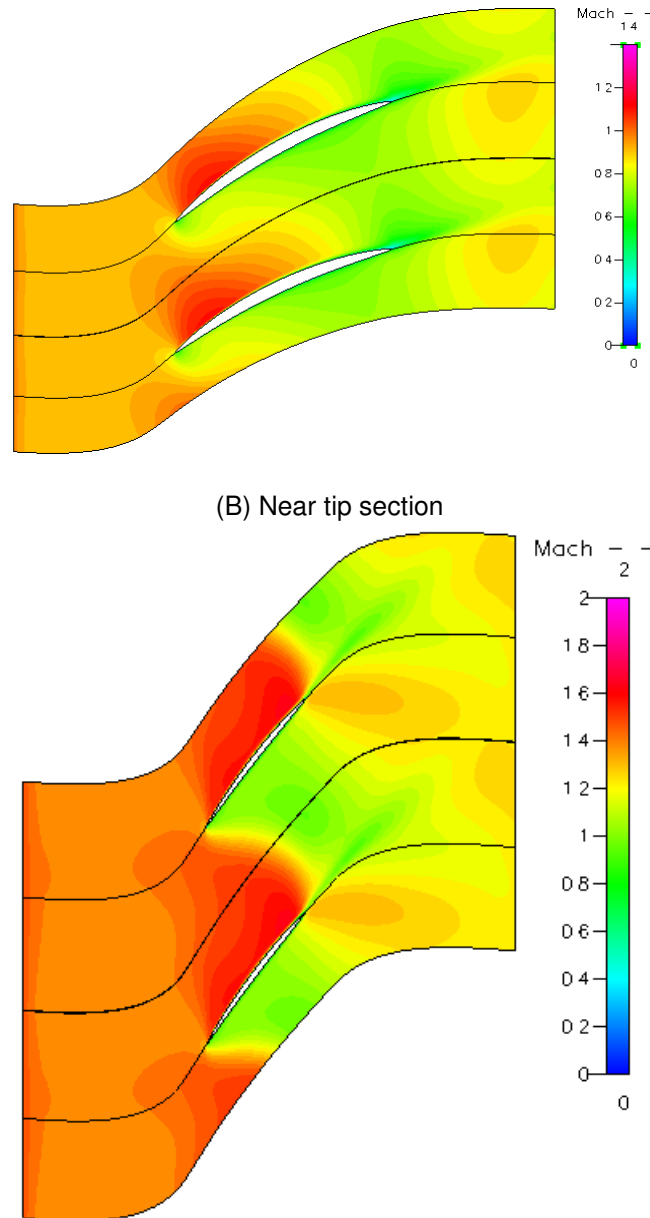


Figure 20: High fidelity design Mach contour

Performance of the high fidelity optimum design during the off design operation is presented in figures 21 and 22. The results show that the total pressure ratio tends to increase with the back pressure to a certain value. As the back pressure is increased more, the rotor stalls. Decreasing the back pressure increases the isentropic efficiency to certain peak point then decreases rapidly near the choke point Fig. 22. The same trend was observed for the different operating speeds but the operation range decreases with the increase in rotor speed. This makes the operating speed to be limited to certain value. The operation range measures the stability of the rotor performance. One of the definitions for the surge margin is that defined by [J.P. Gostelow, K.W. Krabacher, L.H. Smith, Jr., (1968)]. Surge margin depends on the mass flow and the pressure ratio at the operating point. This margin is used to measure the rotor stability. The current design has a 12% surge margin which is a reasonable value compared to high loaded fans. For high loaded rotors, the surge margin varies from 10% to 20% [J.P. Gostelow, K.W. Krabacher, L.H. Smith, Jr., (1968)].

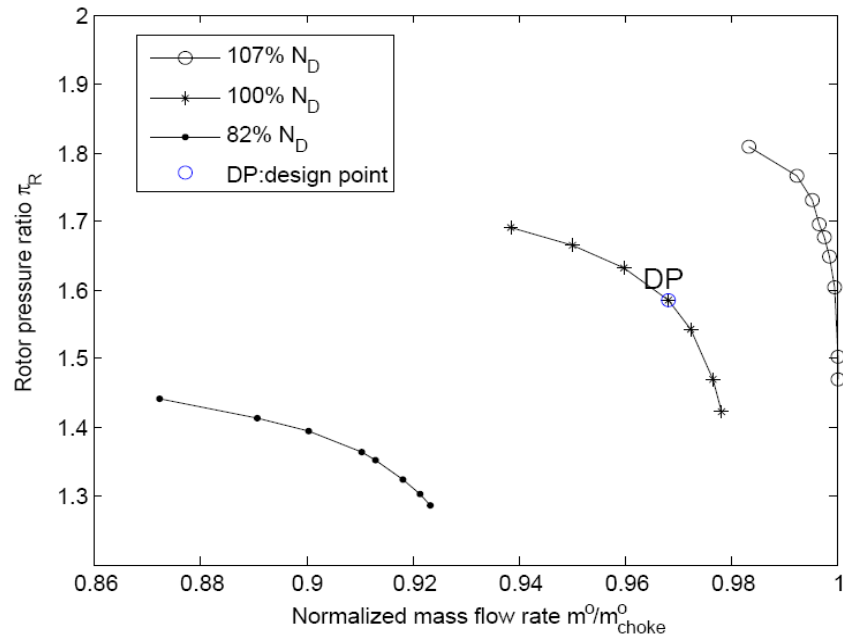


Figure 21: Variation of the total pressure ratio with the mass flow rate at different rotational speeds for high fidelity design.

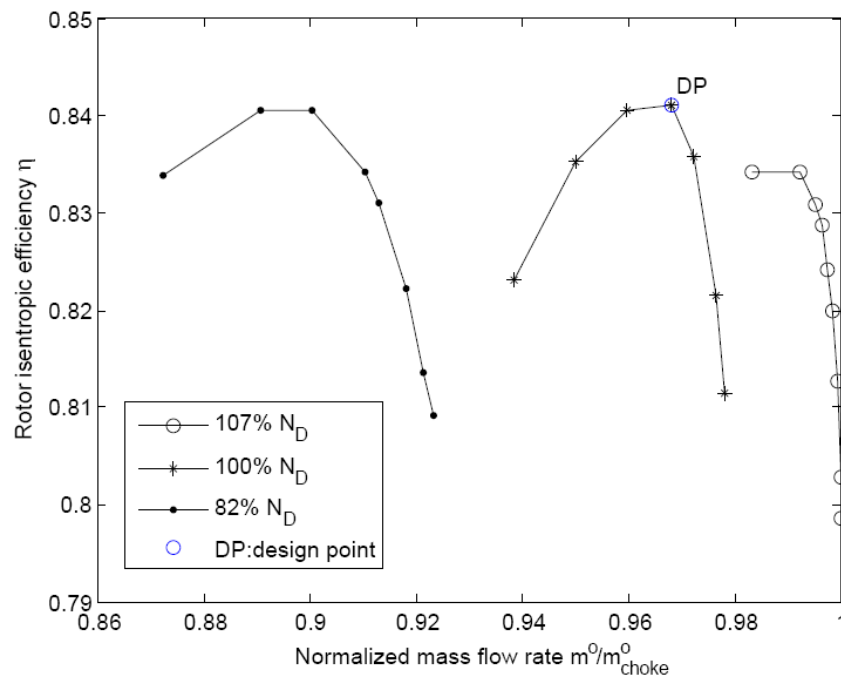


Figure 22: Variation of the isentropic efficiency with the mass flow rate at different rotational speeds.

The shock structure in the transonic compressor passage is very sensitive to the back pressure. There are two regimes for the back pressure controlling the number forming the shock structure which are the low and high back pressure regimes. The range of back pressure for which two distinct passage shocks exist is referred to as the "low back pressure regime". For low back pressure conditions, the passage shock which begins at the blade leading edge is a weak shock and the flow downstream of this shock is supersonic as clear from figure 23 (A). As the back pressure is increased above some "low" value, a normal shock extends across the entire passage and merges with the right branch of trailing edge Figures 24 (B) and 23 (B). This normal shock moves upstream with increasing back pressure and still moving until just coalesce with the first passage shock Figures 24 (C).

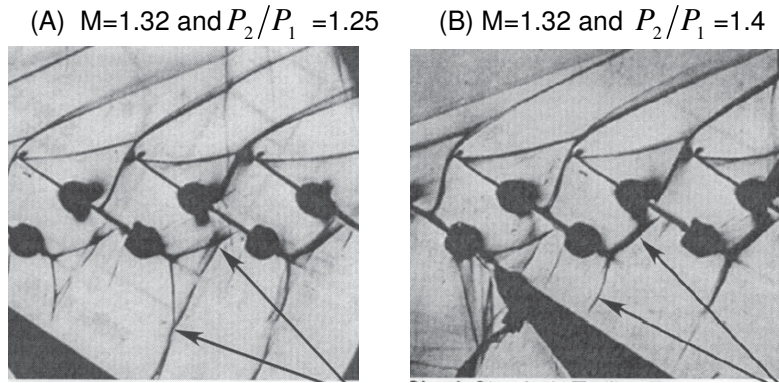


Figure 23: Variation of the second passage shock with back pressure in the low back pressure regime [Gregory S. Bloch, (1996)].

As the back pressure increases, the normal shock continues to move upstream. The passage shock becomes a combination of a weak shock and a full passage normal shock as shown in figure 24 (A). If the back pressure is increased above this maximum value of the "low back pressure regime", the normal passage shock detaches and moves upstream of the blade leading edge. Operating with a detached passage shock is commonly referred to as the "high back pressure" regime. Figures 25 and 26 present the shock structure at the low and high back pressure for high and low design speeds respectively.

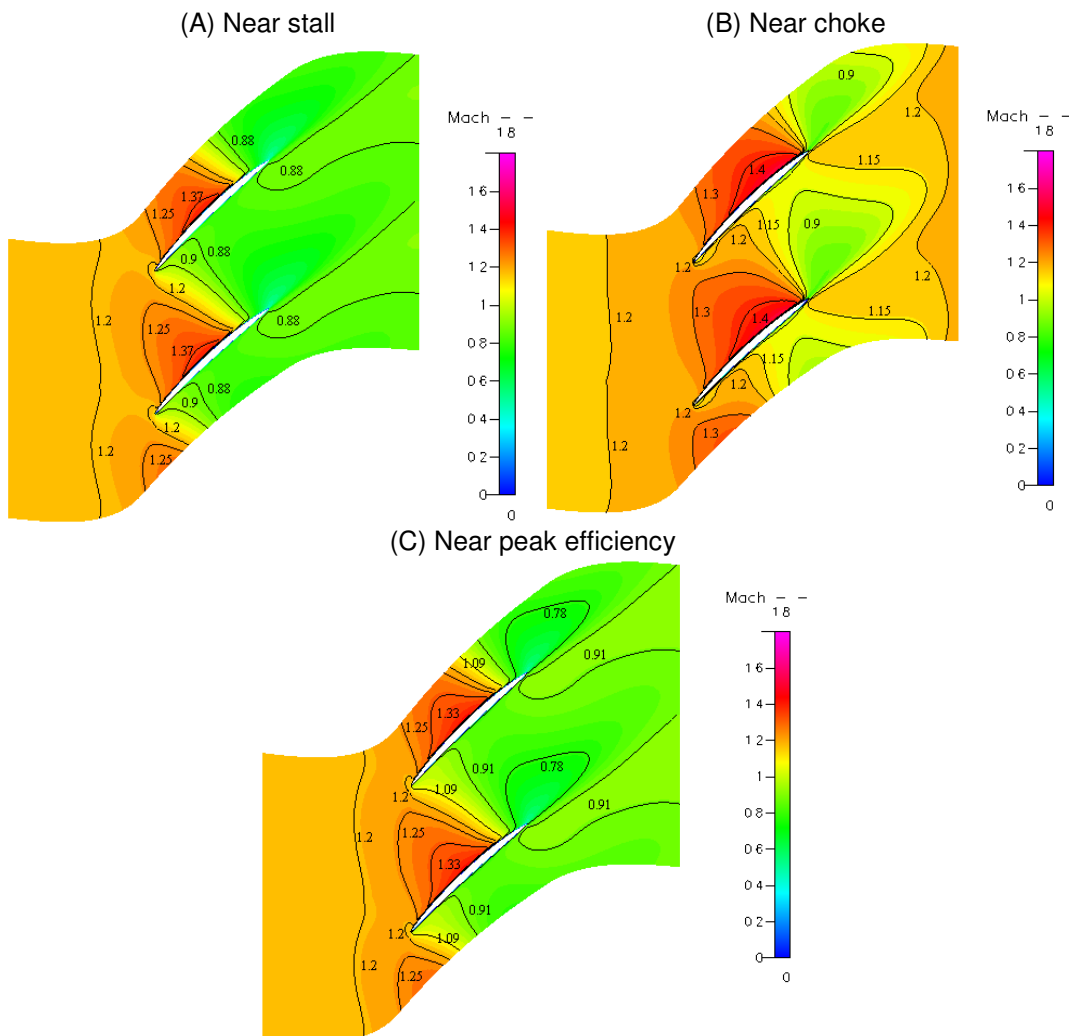


Figure 24: Mach contours for the high fidelity design at the mean section and 100% design speed.

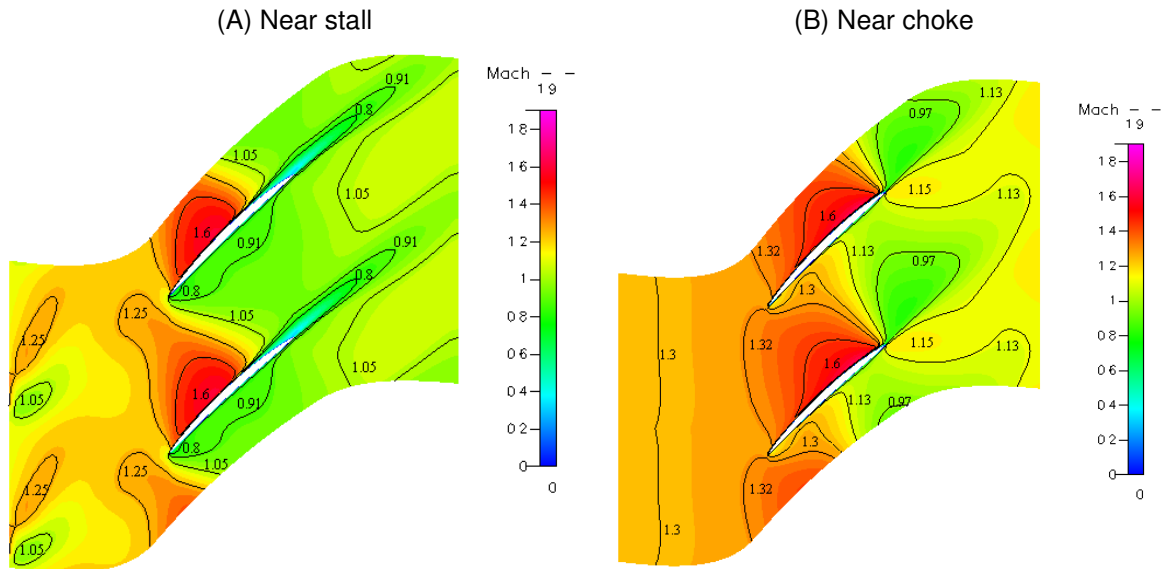


Figure 25: Mach contours for the high fidelity design at the mean section and 107% of the design speed.

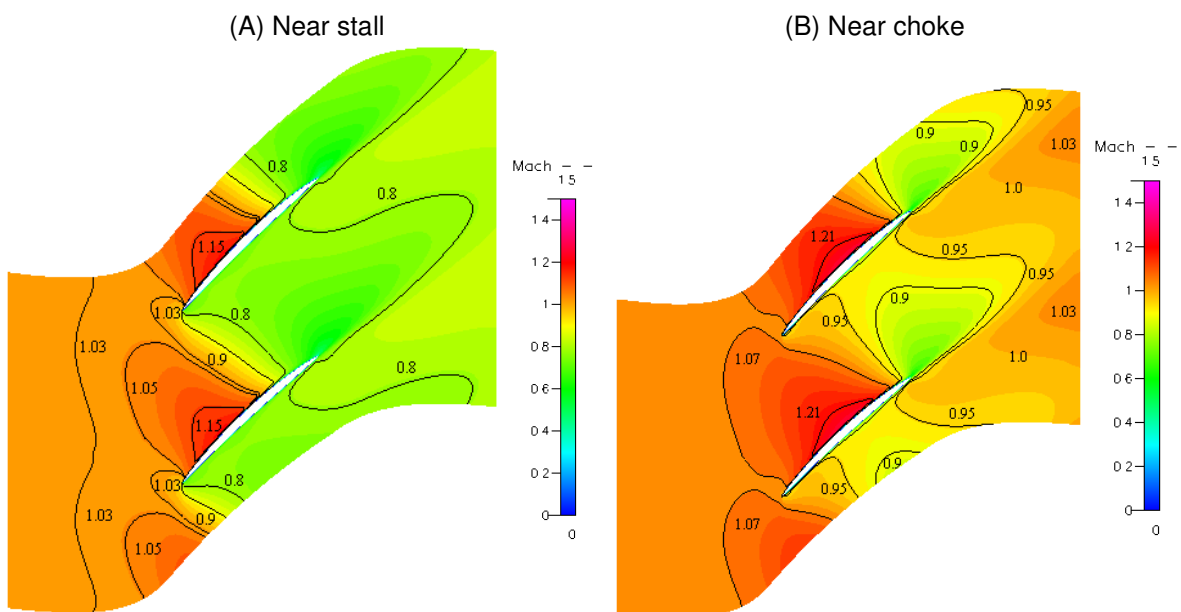


Figure 26: High fidelity design Mach contours at the mean section and 82% design speed.

CONCLUSION

In the current study, the design of a transonic fan is optimized using numerical simulation of the compressible-viscous flow equations and simplex optimization algorithm. The results, obtained using the CFDRC code, are verified with the experimental data of Rotor 67. A grid sensitivity analysis is performed for the numerical simulations. The cost function of the optimization process is the rotor total pressure ratio. The blade geometry is defined in terms of set of optimization groups describing the section chord, stagger angle, staking position, the section thickness and camber distributions. The original total number of variables for the three sections is 84. The optimum design is found to be leaned in the direction of rotation and has a forward sweep from the hub to mean section and backward sweep to the tip. The pressure ratio increases from 1.427 to 1.627 (14%) at the design speed and mass flow rate. The peak efficiency increments were numerically observed using a blade prevalently curved towards the direction of rotation and slightly backward inclined near the tip. A

Fewer number of blades is achieved to reduce the rotor weight. The performance of the new design shows a stable operation during a wide range in the off design.

REFERENCES

Ahn C-S, Kim K-Y., (2002), *Aerodynamic design optimization of an axial flow compressor rotor*. In: Proceedings of ASME turbo expo 2002, GT-2002- 30445.

Benini E, Biollo R., (2007), *Aerodynamics of swept and leaned transonic compressor- rotors*. Applied Energy 0306-2619 2007;84(10):1012–1027 (October 2007).

Benini E, Biollo R., (2008), *Effect of forward and aft lean on the performance of a transonic compressor rotor*. International Journal of Turbo and Jet Engines 0334-0082 2008.

Bergner J, Kablitz S, Hennecke DK, Passrucker H, Steinhardt E., (2005), *Influence of sweep on the 3D shock structure in an axial transonic compressor*. In: Proceedings of ASME turbo expo 2005, GT2005-68835.

BiolloR, Benini E., (2008), *Impact of sweep and lean on the aerodynamic behavior of transonic compressorrotors*. In: Proceedings of the future of gas turbine technology—fourth international conference, 2008a, IGTC08_P17.

Boyce, M.P,(2003), *Gas Turbine Engineering Handbook*. Second Edition, Butterworth-Hienemann 2003.

Choon-Man, PingLI, and Kwang-Yong KIM, (2005), *Optimization of Blade Sweep in a Transonic Axial Compressor Rotor*. JSME International Journal, Series B, Vol.48, No.4, 2005.

Gregory S. Bloch, 1996, *Flow Losses in Supersonic Compressor Cascades*. Doctor of Philosophy, Virginia Polytechnic Institute and State University, Blacksburg, Virginia, july 1996.

Hah C, Puterbaugh SL, Wadia AR., (1998), *Control of shock structure and secondary flow field inside transonic compressor rotors through aerodynamic sweep*. In: Proceedings of the 1998 international gas turbine & aero engine congress & exhibition, 1998, ASME Paper 98-GT-561.

Hah C, Rabe DC, Wadia AR., (2004), *Role of tip-leakage vortices and passage shock in stall inception in a swept transonic compressor rotor*. In: Proceedings of ASME turbo expo 2004, 2004, GT2004-53867.

Hah, C. & Reid, L. (1992), *A Viscous Flow Study of Shock-Boundary Layer Interaction, Radial Transport, and Wake Development in a Transonic Compressor*, ASME Journal of Turbomachinery. Vol. 114, No. 3, pp. 538-547, July 1992.

J.P. Gostelow, K.W. krabacher, L.H. Smith, Jr., (1968), *Performance Comparisons of High Mach Number Compressor Rotor Blading*. National Aerodynamics and Space Administration. Washington, D.C. December, 1968.

- Kablitz S, Passrucker H, Hennecke DK, Engber M., (2003), *Experimental analysis of the influence of sweep on tip leakage vortex structure of an axial transonic compressor stage*. In: Proceedings of 16th symposium on air-breathing engines, ISABE-2003-1226, 2003b.
- Keith M. Boyer, (2001), *An Improved Streamline Curvature Approach for Off-Design Analysis of Transonic Compression Systems*. Doctor of Philosophy, Virginia Polytechnic Institute and State University, Blacksburg, Virginia, April 2001.
- Launder, B. E. and Spalding, D. B., (1972), *Lectures in Mathematical Models of Turbulence*. Academic Press, London, England, 1972.
- Lian, Y., Kim, N.H.,(2005), *Multi-Objective Optimization of Transonic Compressor Blade Using Evolutionary Algorithm*. Journal of Propulsion and Power, Vol. 21, No. 6, pp. 979-987, 2005.
- Lian, Y., Kim, N.H., (2006), *Reliability-Based Design Optimization of a Transonic Compressor*. AIAA Journal, Vol. 44, No. 2, pp. 368-375, 2006.
- Ning, F. & Xu, L., (2001), *Numerical Investigation of Transonic Compressor Rotor Flow Using an Implicit 3D Flow Solver With One-Equation Spalart-Allmaras Turbulence Model*. Proceedings of ASME Turbo Expo 2001, 2001-GT-0359.
- Oyama, A., Liou, L.M., and Obayashi, S. (2002), *Transonic Axial-Flow Blade Shape Optimization Using Evolutionary Algorithm and Three-Dimensional Navier-Stokes Solver*. AIAA 2002-5642.
- Oyama, A., Liou, L.M., and Obayashi, S.,(2003), *High Fidelity Swept and Leaned Rotor Blade Design Optimization Using Evolutionary Algorithm*. AIAA 2003-4091, AIAA Computational Fluid Dynamics Conference, Orlando, FL, 2003.
- Puterbaugh SL, Copenhaver WW, Hah C, Wennerstrom AJ., (1997), *A three-dimensional shock loss model applied to an aft-swept, transonic compressor rotor*. ASME Journal of Turbomachinery 0889-504X 1997;119(3):452–459.
- Qinghai Bai.,(2010), *Analysis of particle swarm optimization algorithm*. Computer and information science, Vol 3, No. 1, February 2010.
- Roache, P.J., (1994), *Perspective: A Method for Uniform Reporting of Grid Refinement Studies*. ASME Journal of Fluid Engineering, Vol. 116, September 1994.
- Roberto Biollo, Ernesto Benini , (2013), *Recent advances in transonic axial compressor aerodynamics*. Progress in Aerospace Sciences journal, 56 (2013) 1–18
- Wadia AR, Copenhaver WW. (1996), *An investigation of the effect of cascade area ratios on transonic compressor performance*. ASME Journal of Turbomachinery 0889-504X 1996;118(4):760–770.
- Wadia AR, Szucs PN, Crall DW., (1998), *Inner workings of aerodynamic sweep*. ASME Journal of Turbomachinery, 0889-504X 1998;120(4):671–682 (October 1998).